Title

SPACE GROUP ANALYSES OF THIN PRECIPITATES BY DIFFERENT CONVERGENT-BEAM ELECTRON DIFFRACTION PROCEDURES

Authors

Howe, J.M.
Sarikaya, M.
Gronsky, R.

Publication Date

1985-08-01

Lawrence Berkeley Laboratory
UNIVERSITY OF CALIFORNIA

Materials & Molecular Research Division

Submitted to Acta Crystallographica, Section A

SPACE GROUP ANALYSES OF THIN PRECIPITATES BY DIFFERENT CONVERGENT-BEAM ELECTRON DIFFRACTION PROCEDURES

J.M. Howe, M. Sarikaya, and R. Gronsky

August 1985

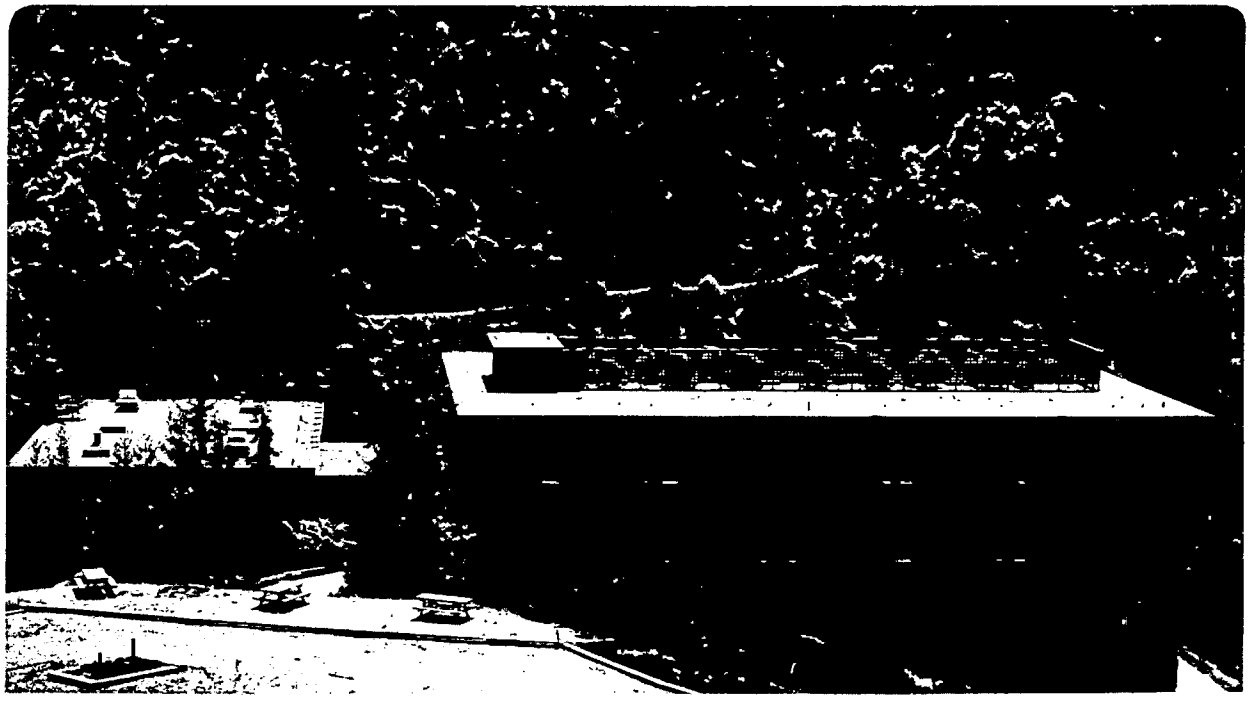

Prepared for the U.S. Department of Energy under Contract DE-AC03-76SF00098

DISCLAIMER

SPACE GROUP ANALYSES OF THIN PRECIPITATES BY DIFFERENT CONVERGENT-BEAM ELECTRON DIFFRACTION PROCEDURES

J.M. Howe

Department of Metallurgical Engineering and Materials Science
Carnegie-Mellon University
Pittsburgh, PA 15213, U.S.A.

M. Sarikaya

Department of Materials Science and Engineering
University of Washington
Seattle, WA 98195, U.S.A.

R. Gronsky

Materials and Molecular Research Division
Lawrence Berkeley Laboratory
and Department of Materials Science and Mineral Engineering
University of California
Berkeley, CA 94720, U.S.A.

ABSTRACT

Convergent-beam electron diffraction point and space group analyses were performed on thin γ' precipitate plates, which had been extracted from an Al-15 w/o Ag alloy aged for either 30 or 120 min. at 350 °C. Although the space groups of precipitates in both samples were determined to be $P6_3/mmc$, it is shown that different results can be obtained, depending on the method of convergent-beam electron diffraction analysis that is employed. Comparative analyses using a pure α-titanium standard demonstrate that the limited thickness of the plate-shaped precipitates is responsible for the variable results, suggesting a preferred method for point and space group determination of thin particles.

1. INTRODUCTION

Howe and Gronsky (1985) recently demonstrated that symmetry determinations performed on thin specimens by convergent-beam electron diffraction (CBED) may reflect the limited thickness of the specimen along the electron-beam direction, rather than the actual space group of the material. This is an important effect, particularly in materials science where many of the microconstituents which strongly influence the properties of engineering materials are only a few-hundred Angstroms thick, a thickness where dynamical diffraction is limited.

This article reports the results of space group determinations which were performed on thin (< 300 Å thick) γ' precipitate plates in an Al-Ag alloy by CBED. Because these plates require both chemical and structural changes for growth, it was hoped that CBED could be used to follow any symmetry or lattice parameter changes which might occur during the early stages of the growth process. Unfortunately, due to the limited thickness of the γ' precipitates, difficulties were encountered which prevented complete determination of some of these factors. Because of these difficulties, both space group and lattice parameter determinations were performed on a pure α-titanium standard for comparison. In order to achieve the most reliable results, different methods for point group determination that have been outlined by Buxton, Eades, Steeds and Rackham (1976), Steeds and Vincent (1983) and Tanaka, Saito and Sekii (1983a) were compared, as were different methods for space group determination that have been outlined by Goodman (1975) and Tanaka, Sekii and Nagasawa (1983b).

Pure α-titanium was chosen as a standard material because it has similar lattice parameters, average atomic scattering factor and space group anticipated for the γ' precipitates. In order to clarify the presentation of the CBED results, the complete space group and lattice parameter determinations for the α-titanium are shown first, followed by the results from the extracted precipitates.

2. EXPERIMENTAL

An aluminum alloy containing 14.92 w/o Ag (4.2 a/o Ag) was vacuum melted and cast using Al and Ag of 99.99% purity. The ingot was subsequently homogenized at 535 °C for about 40 hrs. to reduce segregation and then hot and cold rolled to 7 mil (178 μm) final thickness. Several 12 mm x 12 mm pieces of the sheet were solution annealed for 30 min. at 550 °C, quenched in cold water and then aged for either 10, 30 or 120 min. at 350 °C, followed by a final cold-water quench. The γ' precipitates were extracted from each of these sheets by dissolving the matrix in a 5% NaOH solution and dispersing the precipitates in CH_3OH. A small amount of the CH_3OH was then collected in an eyedropper and a drop or two deposited on a lacy-carbon grid, leaving the γ' plate-shaped precipitates face-down for analysis.

Hot-rolled 32 mil (0.8 mm) thick, 99.99% Ti sheet was ground to 5 mil (125 μm) thickness on water-cooled SiC papers down to 600 grit. Discs 3.0 mm in diameter were punched, vacuum encapsulated and annealed for 1 hr. at 600 °C to produce a completely-recrystallized, α-phase microstructure. Thin foils were prepared by polishing the

discs in a twin-jet Fischione apparatus using a 25% HNO_3/75% CH_3OH electrolyte at about -35 °C, with an applied potential of about 50 V and a current of 50 mA.

All of the CBED experiments were performed on a Philips EM400 analytical microscope operating at 100 kV, and equipped with an external circuit so that the objective lens (OL) and 2nd condenser lens (C2L) currents could be independently controlled to achieve a wide range of incident-probe diameters (~ 100-300 Å) and convergence angles (~ 10-30 mrad) on the specimens (Sarikaya and Thomas 1984). In order to fully utilize the information present within the zero-order Laue zone (ZOLZ) CBED discs, the 1st condenser lens (C1L) was set at the highest excitation (smallest probe diameter) and then the OL current was increased so that the diffraction discs in the ZOLZ just touched without overlapping, while independently focussing the probe on the sample with the C2L "free control". Tilting experiments were performed by translating the C2L aperture (equivalent to a gun tilt), after first having obtained a zone axis (ZA) pattern. A 300 μm C2L aperture and a 450 mm camera length were usually used to photograph the intensity distributions within the ZOLZ discs while a 100 μm C2L aperture and a 280 mm camera length were employed for photographing the first-order Laue zone (FOLZ). A double-tilt, liquid-nitrogen cooled specimen holder (Temp. = -188 °C) was utilized to eliminate contamination and reduce thermal diffuse scattering in the specimens, which then produced sharp CBED patterns.

3. RESULTS

3.1. EXAMINATION OF SPACE GROUP AND LATTICE PARAMETERS OF ∝-TITANIUM

In its ∝-phase form, Ti has a hexagonal close-packed structure with a = 2.95030 Å and c = 4.68312 Å (Boyer and Gall 1985) and is centrosymmetric, with the space group $P6_3/mmc$. All of the CBED pattern symmetry elements for this space group have been derived by Goodman (1975). In addition, Goodman and Whitfield (1980) have performed a complete CBED space group analysis for GaS, which also has the space group $P6_3/mmc$. The same protocal was followed for determinimg the space groups of both the ∝-titanium and extracted precipitates in the present study.

The CBED map of ∝-titanium in Fig. 1 shows the relationship among the zone axes used in these analyses. The zone axes of interest are the [0001] principal zone and the $[1\bar{1}04]$, $[1\bar{1}02]$ and $[3\bar{3}02]$ zones, all of which are reached by rotating the specimen about $\langle 11\bar{2}0\rangle$.

Figure 2 shows several CBED patterns obtained from the [0001] principal zone, with the discs in the FOLZ indexed. Notice that both the whole pattern (WP) and bright field (BF) disc in the ZOLZ patterns shown in Figs. 2(a) and (b) have 6mm symmetry. That is, they possess 6-fold rotational symmetry about an axis which lies in the center of the BF disc (asterisk in Fig. 2(a)) and runs perpendicular to the plane of the figures (electron-beam direction). These patterns also contain two mirror lines oriented horizontally and vertically in the figures. Also notice that the FOLZ shown in Fig. 2(c) displays the same 6mm symmetry. Reference to columns 6 and 7 in Table 2 of Buxton et al. (1976) shows that the only two diffraction groups in

which both the BF disc and WP show 6mm symmetry are 6mm and 6mm1$_R$.

Column 4 in Table 2 of Buxton et al. (1976) shows that it is possible to further distinguish between the diffraction groups 6mm and 6mm1$_R$ by examining the symmetry present within a dark-field (DF) disc when it is located at a "special" position in the pattern. In this case, a <$\bar{1}$010> disc located at its Bragg position on one of the mirror lines in the pattern is in a "special" position and thus, will display only m symmetry if the diffraction group is 6mm, but will display 2mm symmetry if the diffraction group is 6mm1$_R$. Also notice from column 6 in Table 2, that these two diffraction groups can be further distinguished by comparing the intensity distributions between $\pm\vec{g}$ pairs of <$\bar{1}$010> discs when they are set at their respective Bragg positions. These pairs of discs will only be related by a 180° rotation, i.e. 2, if the diffraction group is 6mm, but will be related by a 180° rotation where the detail within each disc also contains perfect inversion symmetry, i.e. 21$_R$, if the diffraction group is 6mm1$_R$. This latter operation is equivalent to a perfect translation between the $\pm\vec{g}$ discs.

Figs. 3(a) and (b) show the intensity distributions within the [$\bar{1}$010] and [10$\bar{1}$0] discs when they are set at their respective Bragg positions. Although the detail within each of these discs displays nearly perfect 2mm symmetry as indicated in the figures, very close inspection reveals that the detail between the tops and bottoms of the discs is slightly asymmetric, which destroys the horizontal mirror in the discs and causes them to be related by a 180° rotation. Thus, the diffraction group of this specimen is 6mm according to the most rigorous analysis of these patterns. However, it is well established

that the correct diffraction group for α-titanium is $6mm1_R$. Thus, it may be concluded that the slight asymmetry which occurs in the $\langle\bar{1}010\rangle$ discs is due to both the limited thickness of the specimen in the area of analysis and to the weak higher-order Laue zone (HOLZ) interactions associated with this high-symmetry zone, as evidenced by the lack of HOLZ lines in the ZA patterns (Howe and Gronsky 1985).

If the point group of this material is then determined by referring to Table 3 in Buxton et al. (1976), an incorrect result is obtained. In Table 3, the diffraction group 6mm yields a corresponding point group of 6mm. The true point group of α-titanium is 6/mmm. Thus, the $\pm\vec{g}$ analysis failed to detect the presence of a horizontal mirror in the sample. Notice that if a similar analysis is performed by reference to Table 2 in Steeds and Vincent (1983) with the use of Table 2 in Buxton et al. (1976) for the $\pm\vec{g}$ or DF symmetries, the same incorect point group is obtained for the α-titanium sample.

Tanaka et al. (1983a) have introduced a slightly different method for determining the diffraction group of a crystal. Their method uses the detail within all of the discs in a single or pair of symmetric many-beam (SMB) patterns in order to obtain the diffraction group. Fig. 3(c) shows a 6-beam pattern from the Ti sample, where the incident beam has been tilted such that the $[\bar{1}010]$ disc is now centered on the optic axis with the [0000] and $[\bar{2}020]$ discs positioned symmetrically on either side. The diffraction group of Ti can be determined directly from this pattern by comparing the detail within the six CBED discs in Fig. 3(c) with the symmetries in the discs in Fig. 3 in Tanaka et al. (1983a) and with Table 3 in the same article. Notice that the $[\bar{2}020]$ disc in Fig. 3(c) displays 2mm symmetry as indicated in the figure,

and that the [0000] disc and four remaining excited discs surrounding the optic axis all have m symmetry. Also notice that the mirror lines in these discs cross the center of the $[\bar{2}020]$ diffracting disc. According to the notation in Fig. 3 of Tanaka et al. (1983a), the $\vec{0}$ and $\vec{G}$ discs correspond to the [0000] and $[\bar{2}020]$, or $2\vec{g}$ disc in Fig. 3(c). Examination of the symmetries in the $\vec{G}$ discs in Fig. 3 shows that the only diffraction group which contains 2mm symmetry is $6mm1_R$, in the lower-right corner. In addition, notice that the $\vec{0}$ disc and four remaining discs in Fig. 3 of Tanaka et al. (1983) all possess m symmetry, where the mirror lines intersect the center of the $\vec{G}$ disc, just as in Fig. 3(c). Thus, it is possible to conclude that the diffraction group of α-titanium is $6mm1_R$ by comparing the single 6-beam pattern in Fig. 3(c) with the schematic many-beam patterns in Fig. 3 of Tanaka et al. (1983a). The same features can also be seen by inspecting the SMB pattern for GaS (space group $P6_3/mmc$) in Fig. 3(b) of Goodman and Whitfield (1980), although these authors do not use these features in their analyses. Also notice the mirror lines in the $\langle\bar{1}010\rangle$ discs in Fig. 3(c) are spaced at 30° intervals around the pattern.

The point group is then found to be 6/mmm from Table 3 in Buxton et al. (1976) by following the same procedure as above. Hence, the Buxton et al. (1976) and Tanaka et al. (1983a) methods for point group determination give different results for the α-titanium sample, the Tanaka et al. (1983a) method yielding the correct result. It is important to note that the Buxton et al. (1976) method would have yielded the same result if the $\pm\vec{g}$ experiment had been performed in a slightly thicker area, since only a slight asymmetry prevented opposite $\langle\bar{1}010\rangle$ discs from having perfect 2mm symmetry and therefore, being

related by a perfect translation operation (2_1^R). Thus, it appears that the SMB technique for diffraction group determination is less sensitive to the limited thickness of the specimen than the $\pm\vec{g}$ technique.

Analysis of mirror lines is further investigated in Fig. 3(d), where a different many-beam pattern was obtained for the Ti sample by tilting the incident-electron beam about the $\langle\bar{1}100\rangle$ axis such that the $[2\bar{1}\bar{1}0]$ and $[\bar{1}2\bar{1}0]$ reflections are equaly excited. Notice that the mirror lines which bisect all of the $\langle 11\bar{2}0\rangle$ discs indicated in the figure are also spaced at 30° intervals around the pattern. This feature indicates the presence of horizontal 2-fold axes at intervals of 60° around the [0001] ZA, parallel to the $\langle 11\bar{2}0\rangle$ directions, as shown in Fig. 3 in Goodman (1975) and Fig. 6(d) in Goodman and Whitfield (1980).

The space group of α-titanium can now be determined by identifying the presence of kinematically forbidden reflections in the CBED patterns. There are only four space groups which have 6/mmm symmetry; P6/mmm, P6/mcc, $P6_3/mcm$ and $P6_3/mmc$, which appear as space group numbers 191 through 194, respectively, in Volume I of the "International Tables for X-ray Crystallography," (Henry and Lonsdale 1976). Examination of the conditions limiting possible reflections for these four space groups indicates that they can be readily distinguished by determining the presence or absence of two types of forbidden reflections: 1) $h\bar{h}0l$, l=2n+1; and 2) $hh2\bar{h}l$, l=2n+1. As summarized in Table 1, space group P6/mmm does not have any forbidden reflections, space groups P6/mcc and $P6_3/mcm$ both contain forbidden reflections of the type $h\bar{h}0l$, l=2n+1 while space group $P6_3/mmc$ has a forbidden reflection of the type $hh2\bar{h}l$, l=2n+1.

In Fig. 2(c), each of the discs which are centered between the pairs of <11$\bar{2}$0> Kossel lines in the FOLZ have dark bands through their centers. One of these bands is indicated by the arrow in Fig. 2(c) and is shown in greater detail in Fig. 2(d), where it is set at the Bragg position. These dark bands or lines of negligible intensity are Gjonnes-Moodie (G-M) lines (Gjonnes and Moodie 1965) and their presence is due to either glide planes or screw axes in the crystal. Gjonnes and Moodie (1965) have determined the conditions under which kinematically forbidden reflections remain at zero intensity when dynamic interactions are included. In the case where the forbidden reflection is due to a vertical glide plane and HOLZ interactions are included, the lines of dynamical absence are present when the incident beam lies in the plane defined by the reciprocal lattice vector of the forbidden reflection. This condition is satisfied for the <11$\bar{2}$1> reflections in Figs. 2(c) and (d), indicating that they are due to a c-glide plane parallel to the electron beam direction. Thus, reflections of the type <11$\bar{2}$1> or hh2$\bar{h}$l, h=2n+1 are forbidden for α-titanium. This eliminates P6/mmm and $P6_3/mcm$ as possible space groups for this material (Table 1).

In order to distinguish between the space groups P6/mcc and $P6_3/mmc$, the sample must be tilted to zone axes where hh$\bar{0}$l, l=2n+1 reflections can be tested for dynamic absences. Reflections of this type occur in both the [3$\bar{3}$02] and [1$\bar{1}$04] zones, and were examined in this study. These zone axes were reached by tilting the sample along a <11$\bar{2}$0> Kossel line pair, as shown in Fig. 1. The exact [3$\bar{3}$02] ZA pattern is shown in Fig. 4(a). Notice that when opposite <$\bar{1}$103> reflections are set at their respective Bragg positions in Figs. 4(b)

and (c), they display strong intensity fringes and HOLZ effects, indicating that they are not kinematically forbidden, i.e. reflections of the type $hh\bar{0}1$, l=2n+1 are allowed. Thus, reference to Table 1 indicates that the only possible space group for α-titanium is $P6_3/mmc$, as expected. Also notice that the detail between the $[\bar{1}\bar{1}03]$ and $[1\bar{1}0\bar{3}]$ discs is related by a perfect translation operation (21_R), which verifies the element of centrosymmetry in the crystal (Buxton et al. 1976, Goodman and Whitfield 1980) that was not detected when the $\pm\vec{g}$ experiment was performed in the higher-symmetry [0001] ZA. Thus, it appears that when the sample is thin along the electron-beam direction, the $\pm\vec{g}$ experiment which is often required for diffraction group determination by either the Buxton et al. (1976) or Steeds and Vincent (1983) methods, is more reliable when performed at low-symmetry zone axes. This is because the amount of electron scattering into HOLZ's increases as the crystal repeat distance in the electron-beam direction decreases, leading to increased dynamical diffraction and thereby, fully revealing the 3-dimensional symmetry of the crystal. The increased electron conentration into HOLZ's is evident by the strong HOLZ lines in the BF disc in Fig. 4(a) as compred to the BF disc in Fig. 2(b).

The $[11\bar{2}0]$ and $[\bar{1}\bar{1}20]$ discs in Figs. 4(d) and (e) are also related by a similar perfect translation operation and in addition, notice that the mirrors in these discs are perpendicular to their reciprocal lattice vectors. This feature indicates the presence of a horizontal 2-fold rotation axis which is parallel to the $\langle 11\bar{2}0\rangle$ axis in the crystal (Goodman and Whitfield 1980), as was observed for Figs. 2(c) and (d). Also notice that the $[33\bar{0}2]$ ZA pattern is nearly square.

This is different from the highly rectangular [$3\bar{3}02$] CBED pattern shown in Fig. 3 of Goodman and Whitfield (1980), indicating that they identified the wrong ZA pattern as [$3\bar{3}02$] in their paper. However, this does not detract from their results.

Fig. 5 shows the [$11\bar{2}4$] CBED ZA pattern and three 4-beam patterns, which were obtained by tilting the incident beam such that it is symmetrically positioned among the four discs, as indicated in the figures. Notice that the intensities within the <$\bar{2}201$> reflections in these patterns are quite strong, and that they do not display evidence of G-M lines, further verifying that $h\bar{h}0l$, l=2n+1 reflections are not forbidden. Also notice that opposite pairs of both <$11\bar{2}0$> and <$\bar{2}201$> reflections in this low-symmetry ZA display perfect translational symmetry as well as the presence of horizontal 2-fold rotation axes. In addition, the detail within the <$\bar{1}\bar{3}21$> CBED discs has almost perfect inversion symmetry (1_R), indicating the presence of a horizontal mirror (/m) in the crystal, i.e. perpendicular to the electron beam (Buxton et al. 1976, Goodman and Whitfield 1980). Thus, all of the symmetry elements for the space group $P6_3/mmc$ have been directly identified from these CBED patterns, exactly as outlined by Goodman (1975) and performed by Goodman and Whitfield (1980) for GaS, except for the 6_3 screw axis, which can only be identified by examining the specimen in either <$11\bar{2}0$> or <$\bar{1}010$> orientations, 90° to the <0001> axis. Since it is not possible to obtain these orientations in this foil or in the extracted precipitates which follow because the basal plane is orientated perpendicular to the electron beam, it is not possible to identify the space group of the samples using Table 13 in

Tanaka et al. (1983b), which requires examination of the G-M lines in either a <11$\bar{2}$0> or <$\bar{1}$010> orientation.

Again, notice the strong HOLZ lines in the [1$\bar{1}$04] ZA pattern in Fig. 5(b) as compared to the <0001> ZA patterns in Figs. 2(a) and (b), where weak HOLZ lines are barely visible. Kohler, Shelton and Ralph (1983) have shown that the fine HOLZ lines in the [1$\bar{1}$04] zone axis vary sensitively with the lattice parameters in hexagonal close-packed crystals and therefore, can be used to make lattice parameter measurements which are accurate up to 0.1%. Thus, the α-titanium is suitable as a standard for this purpose. In addition, the intersection of the Ewald sphere with the FOLZ in Fig. 2(c) leads to a bright ring which can be easily measured to obtain the lattice spacing along the c-axis with an accuracy of about 1% (Steeds and Vincent 1983). This measurement was performed and the lattice parameter along the c-direction was determined to be c = 4.746 Å by using the relation: $G = (2KH)^{1/2}$, where G = radius of the FOLZ ring, K = electron wavevector $(1/\lambda)$, H = reciprocal lattice spacing parallel to the electron beam, and assuming that $d_{\bar{1}010}$ = 2.555 Å. This value for c is about 0.2% larger than the value of 4.68312 Å determined by x-ray diffraction (Boyer and Gall 1985).

3.2. DETERMINATION OF SPACE GROUP AND LATTICE PARAMETERS OF γ' PRECIPITATES

Based on the results from the previous analyses for α-titanium, the present section explains the results of similar space group and lattice parameter determinations which were performed on the extracted γ' precipitates. As previously mentioned, these analyses were performed

in order to follow any symmetry or lattice parameter changes which might occur during the early stages of precipitate growth. However, it was not possible to find any γ' precipitates which were thick enough to display intensity fringes in the CBED discs for the sample which was aged for only 10 min. at 350 °C. In fact, while a number of extracted precipitates could be readily found for analysis in the 120 min. sample, only a few precipitates in the 30 min. sample were thick enough to display any intensity fringes in the CBED patterns. Hence, the effect of precipitate thickening during aging was directly reflected in the CBED analyses, and only precipitates from samples which were aged for times of 30 min. or longer could be examined. In addition, slight distortion of the intensity distributions within the CBED discs from the extracted precipitates sometimes occurred, because the thin precipitates always bent when irradiated by the electron beam. This bending caused the precipitates to be filled with extintion contours (see Fig. 6 for example), and the probe was placed within these bend contours for the CBED analyses. Thus, if the probe was not entirely contained within the zone axis determined by the bend contours, slight distortion of the patterns within the CBED discs resulted.

Figure 7 shows a series of [0001] CBED patterns obtained from a γ' precipitate which was extracted from the sample aged for 30 min. at 350 °C. These patterns can be compared directly with the same series of patterns for the Ti sample in Fig. 2. Although the precipitate is so thin that there is no detail within the BF disc in Fig. 7(b), notice that the WP in Fig. 7(a) and FOLZ in Fig. 7(c) both display 6mm symmetry. Thus, reference to Table 2 in Buxton et al. (1976) shows

that the diffraction group of the precipitate is either 6mm or $6mm1_R$.

Figure 8 shows another series of $\pm\vec{g}$ and tilted-illumination CBED patterns, which may be compared directly with the patterns for the Ti sample in Fig. 3. The $[\bar{1}010]$ and $[10\bar{1}0]$ discs at their Bragg positions in Figs. 8(a) and (b) clearly display only m symmetry as indicated in the figures. In addition, these discs are also related by a 180° rotation, rather than by a perfect translation operation. Thus, reference to Table 2 in Buxton et al. (1976) indicates that the diffraction group for the precipitate which was aged for 30 min. at 350 °C is 6mm, and not $6mm1_R$, just as for the previous Ti sample. By using Table 3 in Buxton et al. (1979), the point group of the precipitate is then identified as 6mm.

If the Tanaka et al. (1983a) 6-beam CBED pattern in Fig. 8(c) is now used to determine the diffraction group of the precipitate instead of the Buxton et al. (1976) method above, a different result is obtained. Although the detail within some of the CBED discs in the SMB pattern is slightly distorted due to bending of the precipitate, the $[\bar{2}020]$ disc displays nearly perfect 2mm symmetry. In addition, the [0000] disc and four remaining excited discs all have m symmetry as indicated in the figure, where the mirror lines intersect the center of the $[\bar{2}020]$ disc. Thus, comparison with the SMB patterns in Fig. 3 of Tanaka et al. (1983a) indicates that the diffraction group of the precipitate is $6mm1_R$, which is the same as the α-titanium sample in Fig. 3(c). Further reference to Table 3 in Buxton et al. (1976) then identifies the point group of the precipitate as 6/mmm.

Thus, the Buxton et al. (1976) and Tanaka et al. (1983a) methods of point group determination yield two different results for the precipitate. Since the Steeds and Vincent (1983) method for point group determination also relies on comparison between the intensity distributions in $\pm\vec{g}$ discs or in a DF disc to distinguish between the 6mm and $6mm1_R$ diffraction groups, the result is the same as with the Buxton et al. (1976) method. However, because both the previous analyses for α-titanium in the [0001] ZA and the centrosymmetry versus thickness results of Howe and Gronsky (1985) for α-titanium in a $\langle 1\bar{1}02\rangle$ ZA have shown that a loss of perfect translational symmetry between $\pm\vec{g}$ discs can occur in thin specimens due only to their limited thickness along the beam direction, it is probable that this effect is responsible for the 180° rotational symmetry observed between the $[\bar{1}010]$ and $[10\bar{1}0]$ discs in Figs. 8(a) and (b), particularly since no HOLZ lines are present in the CBED patterns and the precipitate is just thick enough for weak dynamical diffraction to occur. Thus, it is best to assume that the precipitate has the higher-symmetry diffraction group given by the SMB pattern in Fig. 8(c) and therefore, that its point group is 6/mmm. Also notice that the mirror planes in both Figs. 8(c) and (d) are spaced at 30° intervals in the patterns, indicating the presence of horizontal 2-fold rotation axes at 60° intervals around the [0001] ZA, parallel to the $\langle 11\bar{2}0\rangle$ directions, as for the Ti sample.

The space group of the precipitate is further obtained by identifying the presence of forbidden reflections in the CBED patterns. Assuming that the point group of the precipiitates is 6/mmm, the only four possible space groups are those listed in

Table 1, which can be distinguished by the presence or absence of forbidden reflections of the type $hh\bar{0}1$, $l=2n+1$ and $hh\bar{2}hl$, $l=2n+1$. Notice that G-M lines are present in the $<11\bar{2}1>$ discs in Figs. 7(c) and (d), indicating the presence of $hh\bar{2}hl$, $l=2n+1$ forbidden reflections in the precipitate, exactly as for the α-titanium sample. Thus, the space group of the precipitate must be either $P6_3/mcc$ or $P6_3/mmc$. Again, these two space groups can be distinguished by tilting the precipitate to $[1\bar{1}02]$ and $[1\bar{1}04]$ zone axes, and examining the detail within $<hh\bar{0}1>$, $l=2n+1$ discs.

Figure 9(a) shows the $[1\bar{1}02]$ ZA CBED pattern. Notice that the overall pattern displays 2mm symmetry due to a lack of HOLZ lines, as explained by Howe and Gronsky (1985). These mirror lines are also present in the two sets of $\pm\vec{g}$ pairs shown for the $<11\bar{2}0>$ and $<\bar{1}101>$ reflections in Figs. 9(b) through (d). In particular, notice that the $[\bar{1}101]$ and $[1\bar{1}0\bar{1}]$ discs in Figs. 9(c) and (d) are related by a 180° rotation rather than by a perfect translation operation. This relation was observed between the same pair of discs in thin areas of the α-titanium sample examined by Howe and Gronsky (1985), further indicating that the limited thickness of the precipitate may be responsible for its apparent loss of the /m symmetry element. The limited thickness of the precipitate is evidenced by the lack of detail within these discs due to the weak dynamical diffraction which is occurring. Also notice that there is no evidence of G-M lines in the $<\bar{1}101>$ discs, indicating that $hh\bar{0}1$, $l=2n+1$ reflections are allowed for the precipitate and therefore, that its space group is $P6_3/mmc$, as for the α-titanium sample.

Figure 10 shows the [$1\bar{1}04$] CBED ZA pattern and three 4-beam patterns which can be compared directly with the same series of micrographs for the α-titanium sample in Fig. 5. Notice the resemblance between the detail within the the <$\bar{2}201$> discs in Figs. 5 and 10. The strong intensities of these reflections and lack of evidence that they are forbidden further verifies that $hh\bar{0}1$, $l=2n+1$ reflections are allowed for the precipitate and that its space group is $P6_3/mmc$. In addition, notice that there is almost perfect translational symmetry between opposite <$\bar{2}201$> and <$11\bar{2}0$> reflections in the 4-beam patterns and that these reflections also demonstrate the presence of horizontal 2-fold rotation axes in the precipitate. Further, the detail within the <$\bar{1}3\bar{2}1$> discs has almost perfect inversion symmetry (1_R), indicating the presence of a horizontal mirror (/m) in the precipitate. Thus, as for the previous α-titanium sample, the symmetries obtained from the CBED patterns in this low-symmetry ZA appear to be less sensitive to the limited thickness of the precipitate than the patterns obtained in the previous orientations. The evidence for a center of symmetry and horizontal mirror obtained in this orientation also confirms that the space group of the precipitate is $P6_3/mmc$ and therefore, that the correct point group is 6/mmm as determined by the SMB pattern in Fig. 8(c).

The reason why the [$1\bar{1}04$] ZA reveals the true symmetry elements in thinner specimens is again due to the fact that HOLZ interactions are stronger in this orientation than in the [0001] and [$1\bar{1}02$] orientations, as evidenced by the presence of HOLZ lines within the BF disc in Fig. 10(b). However, these HOLZ lines are still not strong enough to obtain accurate lattice parameter information for the precipitate by comparing

their positions with those in the Ti standard. Nevertheless, by measuring the diameter of the bright ring in the FOLZ (which is barely visible in Fig. 7(c)) and assuming that $d_{\bar{1}010} = 2.477$ Å for the γ' precipitate, the lattice spacing along the c-direction can be determined. Using the equation given above for the titanium sample, a value of c = 4.676 Å was obtained. This spacing is about 1.5% larger than the value of 4.607 Å usually given for these precipitates (Mondolfo 1979, Barrett and Geisler 1940), and is equal to the lattice spacing of two {111} matrix planes, i.e. $d_{111} = 2.338$ Å. One reason for this spacing is that the precipitates are probably less than 200 Å thick and still in the early stages of growth. Thus, they may not have achieved the full contraction along the c-direction which is characteristic of latter stage precipitates. However, Howe, Aaronson and Gronsky (1985a) have measured the lattice spacings of the same precipitates by optical diffraction from HREM negatives, and their results showed that there is about a 2.5% contraction among the basal planes in the precipitates when compared with the octahedral matrix planes. Thus, the larger c-spacing obtained from the CBED pattern is probably more likely due to the error made in measuring the diameter of the FOLZ, since the bright ring associated with the FOLZ is barely visible in the pattern.

Identical space group analyses and lattice parameter determinations were also performed on extracted precipitates from the sample which was aged for 120 min. at 350 °C. The results from from one precipitate are shown in Figs. 11 through 13. Since they are basically identical with those just discussed, only the differences between the analyses for the 30 and 120 min. precipitates are described.

The [0001] CBED patterns for the 120 min. precipitate in Figs. 11 and 12 are similar to those in Figs. 7 and 8, except that detail is present within the BF disc for the precipitate in Fig. 11(b). However, notice that the hexagon within the BF disc does not have 6-fold rotational symmetry. This is due to the fact that the electron probe was focussed slightly above the specimen when the CBED pattern was taken and thus, the detail is slightly elongated in one direction. Therefore, it can be concluded that the BF disc possesses 6mm symmetry when the probe is correctly focussed, and that the diffraction group of this precipitate is either 6mm or $6mm1_R$.

Examination of Figs. 12(a) through (c) again shows that the SMB technique for point group determination (Fig. 12(c)) yields a higher-symmetry point group than the $\pm\vec{g}$ technique (Figs. 12(a) and (b)). The mirror lines in the 6-beam pattern are accurate to a high degree in Fig. 12(c), and clearly indicate that the point group of the precipitate is $6mm1_R$ when compared with Fig. 3 in Tanaka et al. (1983a). Thus, the SMB CBED technique developed by Tanaka et al. (1983a) appears to be preferred over the $\pm\vec{g}$ method of Buxton et al. (1976) and Steeds and Vincent (1983) for determining the point group of thin specimens. In addition, notice that G-M lines are present in the $\langle 11\bar{2}1\rangle$ discs in the FOLZ in Figs. 11(c) and (d), while there is no evidence in Figs. 13(b), (c) and (e) that reflections of the type $hh\bar{0}1$, $l=2n+1$ are forbidden. The detail within these discs is also similar to that observed for both the α-titanium and 30 min. precipitate and thus, it can be concluded that the space group of this precipitate, which was aged for 120 min. at 350 °C, is also $P6_3/mmc$.

The lattice parameter along the c-direction was also calculated for this precipitate from the diameter of the bright ring in the FOLZ in Fig. 11(c). By assuming that $d_{\bar{1}010}$ = 2.477 Å and using the same equation as before, the spacing was found to be c = 4.624 Å. This is about 0.4% larger than the value of 4.607 Å which was determined by x-ray diffraction (Barrett and Geisler 1940), but agrees with these results within the accuracy of the present measurements.

4. DISCUSSION

It is worthwhile to compare the results from the present CBED space group analyses of the γ' precipitates which were aged for 30 min. at 350 °C, with an ordered model structure previously proposed for the same γ' precipitates by Howe, Aaronson and Gronsky (1985b). The present analyses determined the space group of these precipitates to be $P6_3/mmc$. This space group represents a disordered hexagonal close-packed crystal, where the two-atom, unit-cell basis is randomly occupied by either Ag or Al. The model for γ' precipitates proposed by Howe et al. (1985b) based mainly on conventional electron diffraction information, high-resolution electron microscopy (HREM) and image simulations, possesses long-range order among alternate basal planes where every other plane is Ag-rich, and possible short-range order within the Al-rich basal planes. As explained below, there are two possible reasons for the discrepancy between the present CBED results and the previous results of Howe et al. (1985b).

First, Hren and Thomas (1963) observed that γ' precipitates are initially ordered during the early stages of growth at 350 °C, but that these precipitates subsequently disorder during the later stages of

growth, as evidenced by the disappearance of the <0001> reflections. Unfortunately, these authors did not specify the times involved for this reaction. Howe et al. (1985b) also reported that some of the γ' precipitates in their study appeared to be disordered after aging for 30 min. at 350 °C, although most of the precipitates displayed some degree of long-range order among alternate basal planes. Since only the coarsest γ' precipitates from the 30 min. aging treatment were suitable for analysis by CBED, it is likely that these precipitates were undergoing the disorder transformation described by Hren and Thomas (1963), thus yielding the space group $P6_3/mmc$ in the CBED analyses.

Another possible but less likely explanation for the different results is that the order was not detected in the CBED analyses due to the limited thickness of the extracted γ' precipitates analyzed. In his study of β-Si_3N_4, Bando (1983) found that CBED patterns from thin crystals were not sensitive to the weak antisymmetric part of the noncentrosymmetric crystal structure due to the low atomic number of the N atoms. This resulted in an apparent /m symmetry element in the space group because the CBED patterns depended mainly on the crystal potential of the Si atom arrangement. Since there is also a large difference between the atomic scattering factors of Ag and Al, it is possible that the CBED patterns from the thin precipitates examined in this study were not sensitive to the preferred distribution of the weaker scattering Al atoms on alternate basal planes. However, notice that the amplitude of the <0001> reflection in Fig. 14 increases proportionally with the amplitudes of the other first-order beams in an ordered hexagonal close-packed precipitate. Since the precipitates

from the 30 min. sample were thick enough for some dynamical diffraction to cause intensity fringes within the CBED discs in the ZOLZ, they were probably only slightly thicker than one extinction distance for the first-order ZOLZ beams. Although the periodicity of the <0001> beam is almost double the periodicities of the other first-order beams, its amplitude is great enough at this thickness that it should have contributed sufficiently to the dynamic intensities to alter the CBED pattern symmetries if the precipitates were ordered. In addition, since the /m symmetry element in this investigation was present in the $<1\bar{1}04>$ orientations where HOLZ lines were visible in the FOLZ discs for both the 30 and 120 min. precipitates, there should have been sufficient dynamical interactions to reveal the actual symmetries of these specimens. Thus, this explanation does not seem as likely as the disordering reaction described above.

5. SUMMARY

The Tanaka et al. (1983a) method for diffraction group determination by SMB CBED patterns appears to be less sensitive to the limited thickness of specimens than the $\pm\vec{g}$ method, which is used to test for a center of symmetry in both the Buxton et al. (1976) and Steeds and Vincent (1983) procedures. Thus, it appears that the Tanaka et al. (1983a) SMB method is preferred for point group determination of thin specimens. In addition, when the specimen is thin along the electron-beam direction, the $\pm\vec{g}$ test for centrosymmetry is most reliable when performed at low-symmetry zone axes, since HOLZ interactions are generally stronger. In this investigation, the space group of γ' precipitates which were aged for 30 and 120 min. at 350 °C was

determined to be $P6_3/mmc$. Since this space group represents a disordered hexagonal close-packed lattice, the CBED results do not agree with conventional diffraction data and HREM images and simulations (Howe et al. 1985b), which indicate that γ' precipitates aged for 30 min. at 350 °C are largely ordered. While it is possible that the CBED technique may not be sensitive to the order within the precipitates due to their limited thickness along the beam direction, a more likely explanation for this difference is that the γ' precipitates are undergoing a disordering reaction at 350 °C as described by Hren and Thomas (1963), and that the CBED analyses sampled only the thickest and most disordered precipitates. Lattice parameter determinations of the c-spacing in well-developed γ' precipitates performed by measuring the diameter of the FOLZ ring agree with the results of previous x-ray studies (Barrett and Geisler 1940) within the accuracy of the technique employed.

ACKNOWLEDGEMENTS

This work was supported by the Director, Office of Energy Research, Office of Basic Energy Science, Materials Science Division of the U.S. Department of Energy under Contract No. DE-AC03-76SF00098.

REFERENCES

Bando Y. (1983). Acta Cryst. B39, 185.

Barrett C.S. and Geisler A.H. (1940). J. Appl. Phys. 11, 733.

Boyer H.E. and Gall T.L., Eds. (1985). "Metals Handbook - Desk Edition," American Society for Metals, Metals Park, Ohio, p. 1.48.

Buxton B.F., Eades J.A., Steeds J.W. and Rackham G.M. (1976). Phil. Trans. Roy. Soc. London, Ser. A 281, 171.

Gjonnes J. and Moodie A.F. (1965). Acta Cryst. 19, 65.

Goodman P. (1975). Acta Cryst. A31, 804.

Goodman P. and Whitfield H.J. (1980). Acta Cryst. A36, 219.

Henry N.F.M. and Lonsdale K., Eds. (1976). "International Tables for X-ray Crystallography - Vol. I," The Kynoch Press, Birmingham, England, p. 487.

Howe J.M. and Gronsky R. (1985). Ultramicroscopy, in press.

Howe J.M., Aaronson H.I. and Gronsky R. (1985a). Acta Metall. 33(4), 649.

Howe J.M., Aaronson H.I. and Gronsky R. (1985b). submitted to Phil. Mag.

Hren J.A. and Thomas G. (1963). Trans. Met. Soc. AIME 227, 308.

Kohler V.L., Shelton C.G. and Ralph B. (1983). in "Proc. 41st Annual Conf. Elec. Micros. Soc. Amer.," San Francisco Press, San Francisco, Calif., p. 258.

Mondolfo L.F. (1979). "Aluminum Alloys - Structure and Properties," Butterworths, London, p. 213.

Sarikaya, M. and Thomas, G. (1984). "Analytical Electron Microscopy," San Francisco Press, San Frncisco, Calif., p. 97.

Steeds J.W. and Vincent R. (1983). J. Appl. Cryst. 16, 317.

Tanaka M., Saito R. and Sekii H. (1983a). Acta Cryst. A39, 357.

Tanaka M., Sekii H. and Nagasawa T. (193b). Acta Cryst. A39, 825.

TABLES

Table 1. Summary of forbidden reflections for space groups 191-194.

Space Group (Number)	Kinematically Forbidden Reflections
P6/mmm (191)	None
P6/mcc (192)	$h\bar{h}0l$, l=2n+1 and $hh2\bar{h}l$, l=2n+1
$P6_3/mcm$ (193)	$h\bar{h}0l$, l=2n+1
$P6_3/mmc$ (194)	$hh2\bar{h}l$, l=2n+1

FIGURE CAPTIONS

Fig. 1. Partial CBED map for α-titanium around the [0001] principal zone.

Fig. 2. CBED patterns for α-titanium in a [0001] orientation showing: (a) 6mm symmetry of the intensity fringes within the ZOLZ discs, (b) detail within the BF disc, (c) 6-fold symmetry of the FOLZ, and (d) G-M line in the <11$\bar{2}$1> FOLZ reflection at the Bragg position. The location of the optic axis is indicated by an asterisk in these and all subsequent CBED patterns.

Fig. 3. CBED patterns for α-titanium in a [0001] orientation showing: (a) and (b) nearly perfect 2mm symmetry within the [$\bar{1}$010] and [10$\bar{1}$0] discs located at their Bragg positions, respectively, (b) mirror lines in the 6-beam pattern with the [$\bar{1}$010] reflection centered on the optic axis (asterisk), and (d) symmetric excitation of the [$\bar{1}\bar{2}$10] and [$\bar{2}\bar{1}$10] reflections with mirror lines in all the <11$\bar{2}$0> (and <$\bar{1}$010>) discs spaced at 30° intervals.

Fig. 4. (a) [$\bar{3}$302] CBED pattern for α-titanium, (b) and (c) intensity fringes and HOLZ lines within the [$\bar{1}$103] and [1$\bar{1}\bar{0}\bar{3}$] discs at their respective Bragg positions, and (d) and (e) intensity distributions within the [11$\bar{2}$0] and [$\bar{1}\bar{1}$20] discs at their respective Bragg positions. The mirror lines are indicated in all of the Bragg reflections, which also display perfect translational symmetry.

Fig. 5. (a), (c) and (d) Three conjugate 4-beam CBED patterns around the $[1\bar{1}04]$ zone axis shown in (b). Notice the translational symmetries between opposite CBED reflections and the nearly perfect inversion symmetry within the $<\bar{1}3\bar{2}1>$ discs in these patterns. Also notice the strong HOLZ lines in the zone axis pattern in (b).

Fig. 6. Bright-field transmission electron microscope image of two γ' precipitates lying face-down on a lacy-carbon grid. Notice the bend contours (arrows) present throughout the thin precipitates.

Fig. 7. CBED patterns from extracted γ' precipitate in a [0001] orientation showing: (a) 6mm symmetry of the intensity distributions in the ZOLZ discs, (b) absence of detail within the BF disc due to the thinness of the precipitate, (c) 6-fold symmetry of the FOLZ, and (d) G-M line in the $<11\bar{2}1>$ FOLZ reflection at the Bragg position. As for the Ti sample, the position of the optic axis is indicated by an asterisk in all of the CBED patterns.

Fig. 8. CBED patterns for extracted γ' precipitate in a [0001] orientation showing: (a) and (b) a single mirror line and 180° rotational symmetry between the $[\bar{1}010]$ and $[10\bar{1}0]$ discs located at their Bragg positions, respectively, (c) mirror lines in the 6-beam pattern with the $[10\bar{1}0]$ disc centered on the optic axis (asterisk), and (d) symmetric excitation of the $[\bar{1}2\bar{1}0]$ and $[2\bar{1}\bar{1}0]$ reflections with mirrors in all the $<11\bar{2}0>$ (and $<\bar{1}010>$) discs spaced at 30° intervals.

Fig. 9. (a) $[1\bar{1}02]$ CBED pattern for γ' precipitate with 2mm symmetry, (b) and (c) intensity distributions in the $[11\bar{2}0]$ and $[\bar{1}\bar{1}20]$ discs at their respective Bragg positions, and (d) and (e) intensity fringes within the $[\bar{1}101]$ and $[1\bar{1}\bar{1}01]$ discs at their respective Bragg positions. Notice that opposite $\langle\bar{1}101\rangle$ discs in (d) and (e) are related by a 180° rotation.

Fig. 10. (a), (c) and (d) Three conjugate 4-beam CBED patterns around the $[1\bar{1}04]$ zone axis shown in (b). As for the Ti sample, notice the translational symmetries between opposite CBED reflections and the nearly perfect inversion symmetry within the $\langle\bar{1}\bar{3}21\rangle$ discs in these patterns. Also notice the weak HOLZ lines in the zone axis pattern in (b).

Fig. 11. CBED patterns from 120 min. γ' precipitate in a [0001] orientation showing: 6mm symmetry in the ZOLZ, (b) 6-fold symmetry within the BF disc, which is elongated because the probe is focussed slightly above the precipitate surface, (c) 6mm symmetry in the FOLZ, and (d) G-M line in the $\langle 11\bar{2}1\rangle$ FOLZ reflection at the Bragg position. The position of the optic axis is indicated by an asterisk in all of the CBED patterns. The bright ring in the FOLZ is just visible in (c).

Fig. 12. CBED patterns for 120 min. γ' precipitate in a [0001] orientation showing: (a) and (b) a single mirror line and 180° rotational symmetry between the $[\bar{1}010]$ and $[10\bar{1}0]$ discs located at their Bragg positions, (c) mirror lines in the 6-beam pattern with the $[10\bar{1}0]$ disc centered on the optic

axis (asterisk), and (d) symmetric excitation of the $[\bar{1}\bar{2}\bar{1}0]$ and $[2\bar{1}\bar{1}0]$ reflections with mirror lines in all the $<11\bar{2}0>$ (and $<\bar{1}010>$) discs spaced at 30° intervals.

Fig. 13. (a) $[1\bar{1}04]$ zone axis pattern for 120 min. γ' precipitate, (b) 4-beam pattern showing mirrors in the $[\bar{1}\bar{1}20]$ and $[220\bar{1}]$ discs and the inversion symmetry in the $[\bar{1}3\bar{2}\bar{1}]$ disc, (d) $[1\bar{1}02]$ zone axis CBED pattern which has 2mm symmetry but is slightly distorted due to a minor off-focus condition, and (c) and (e) opposite $<\bar{1}101>$ reflections at their respective Bragg positions. Notice that the intensity fringes in the opposite $<\bar{1}101>$ discs have 180° rotational symmetry, but that the faint HOLZ lines which are nearly horizontal in these discs are slightly concave down in both discs, indicating some translational symmetry.

Fig. 14. Amplitudes of the forward-scattered (0000) beam and all of the first-order precipitate reflections as a function of crystal thickness for an ordered Ag_2Al γ' precipitate which contains pure Ag on the A basal planes and 33 a/o Ag on the B basal planes. The amplitudes were normalized by dividing by the sum of the amplitudes.

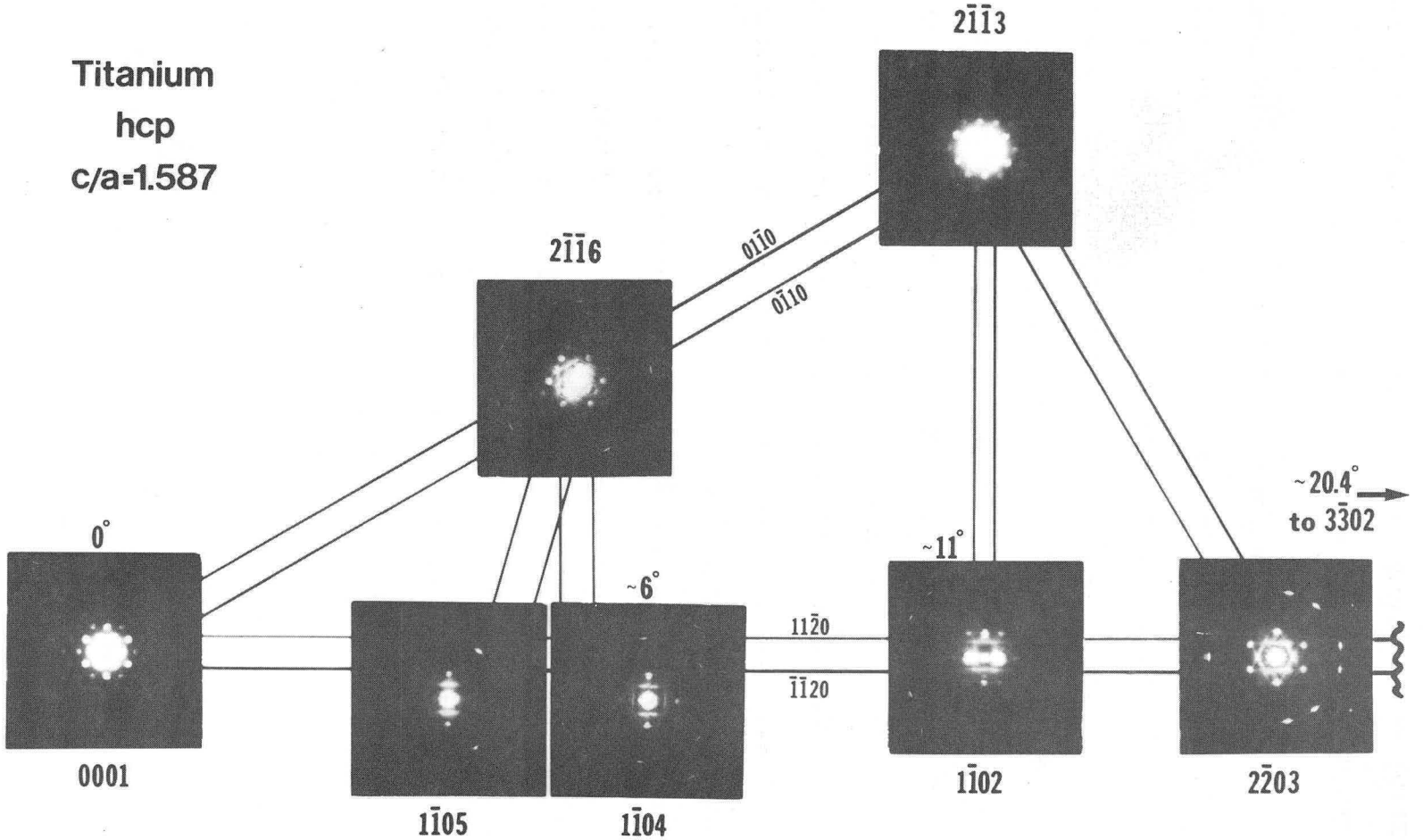
Titanium
hcp
c/a=1.587
$2\bar{1}\bar{1}3$
$2\bar{1}\bar{1}6$
$01\bar{1}0$
$0\bar{1}10$
0°
~6°
~11°
~20.4°
to $3\bar{3}02$
$11\bar{2}0$
$\bar{1}\bar{1}20$
0001
$1\bar{1}05$
$1\bar{1}04$
$1\bar{1}02$
$2\bar{2}03$
XBB 838-7189

Fig. 1

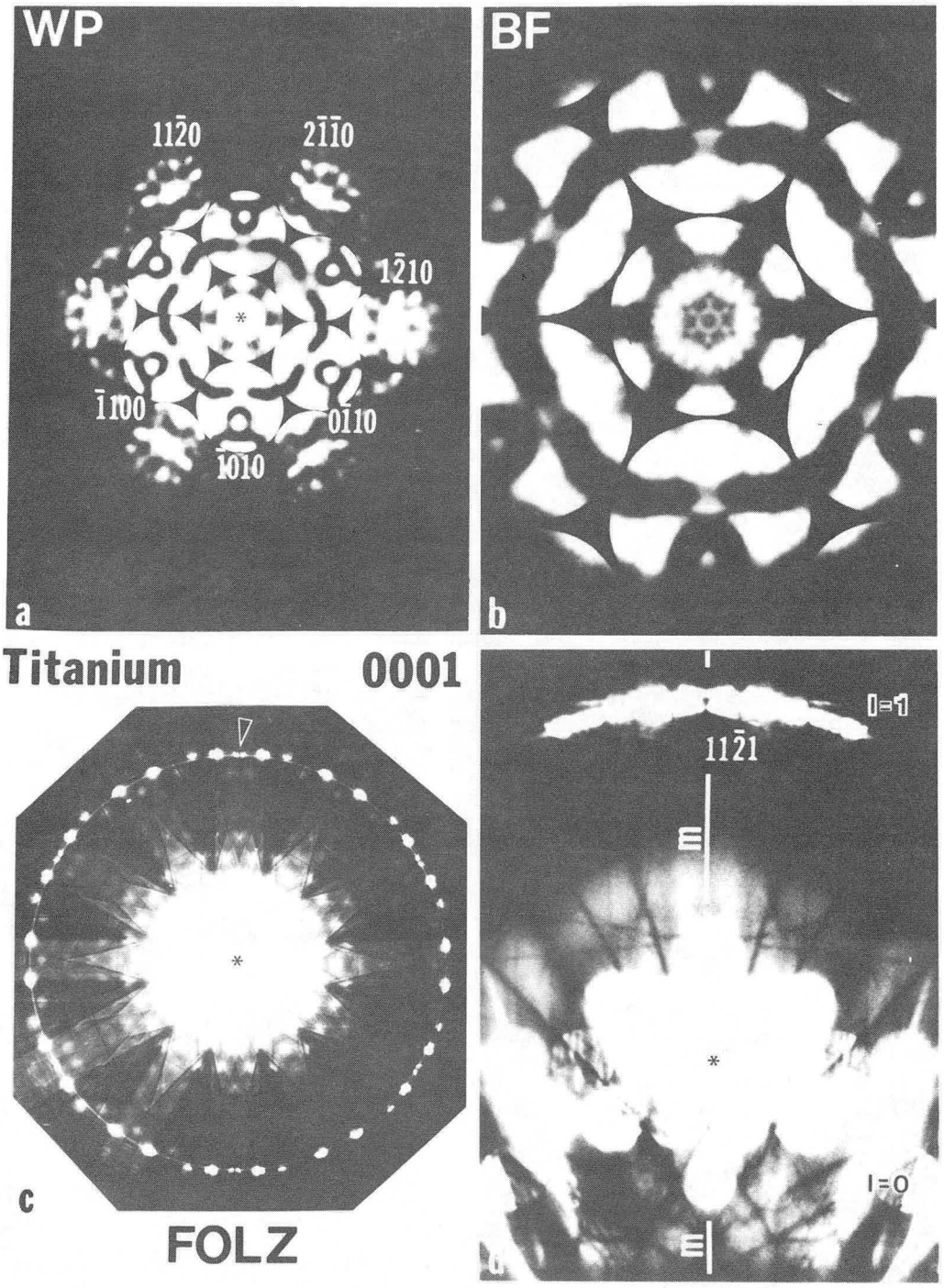

XBB 840-7662

Fig. 2

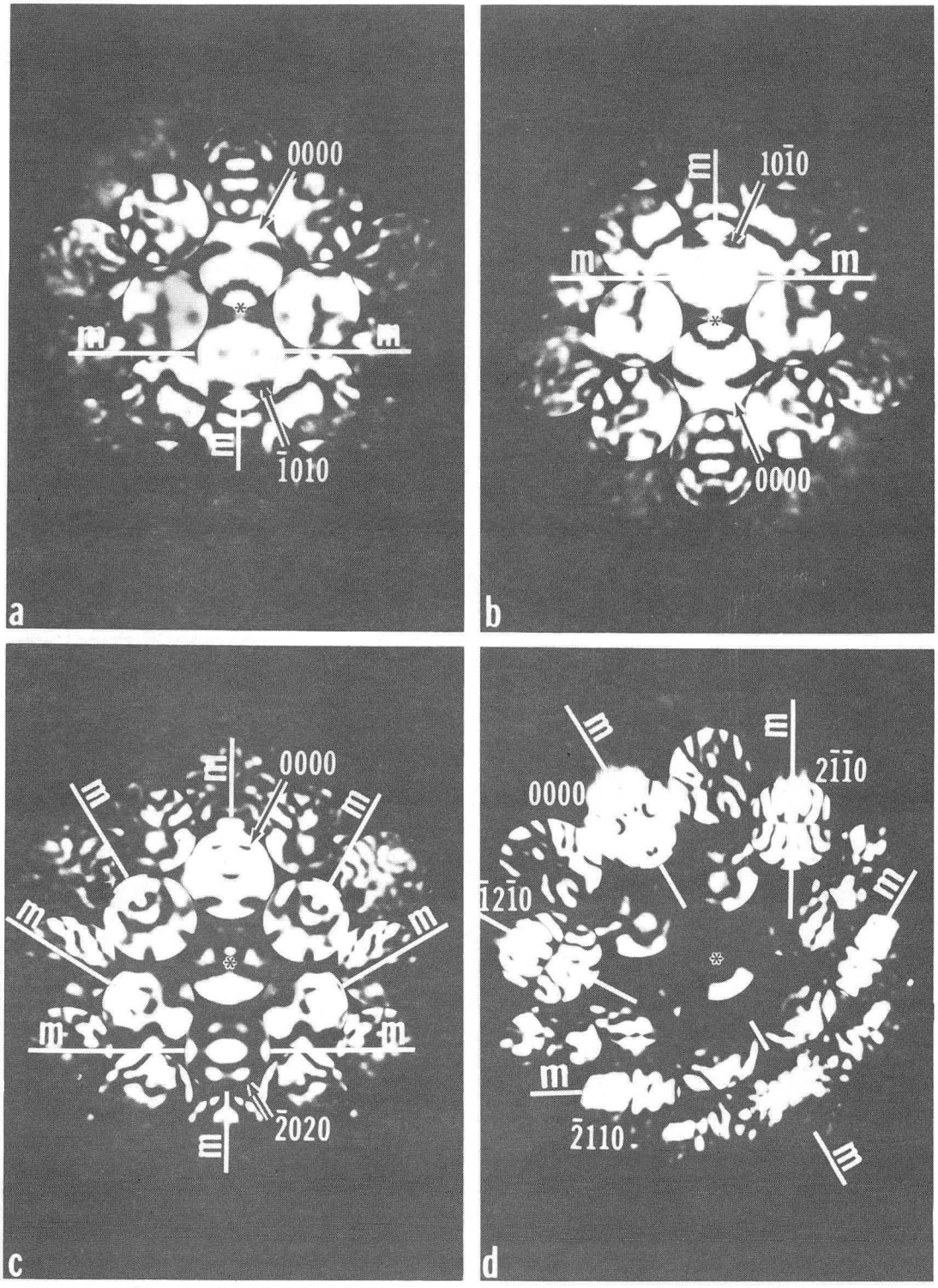

XBB 840-7655

Fig. 3

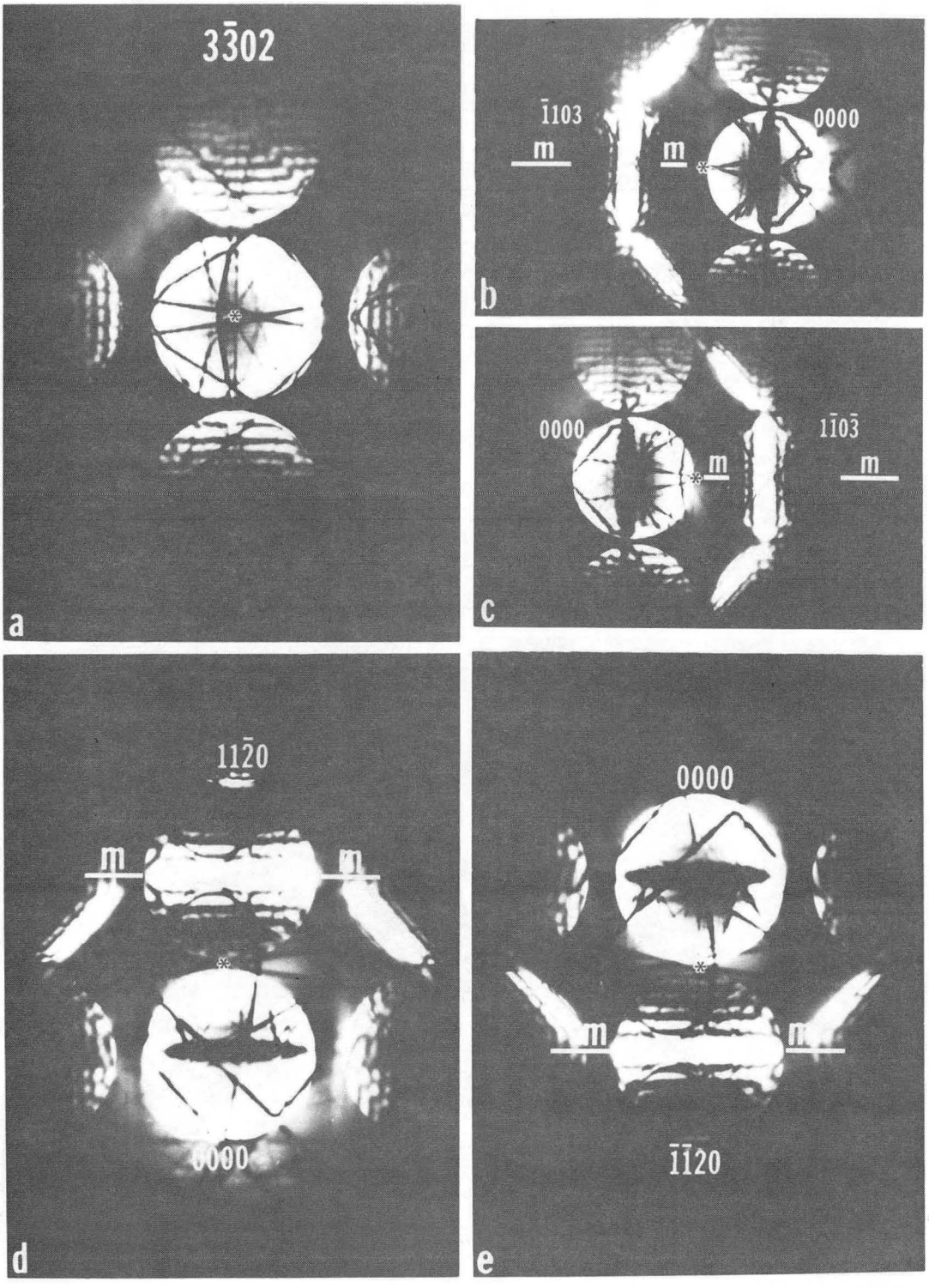

XBB 840-7658

Fig. 4

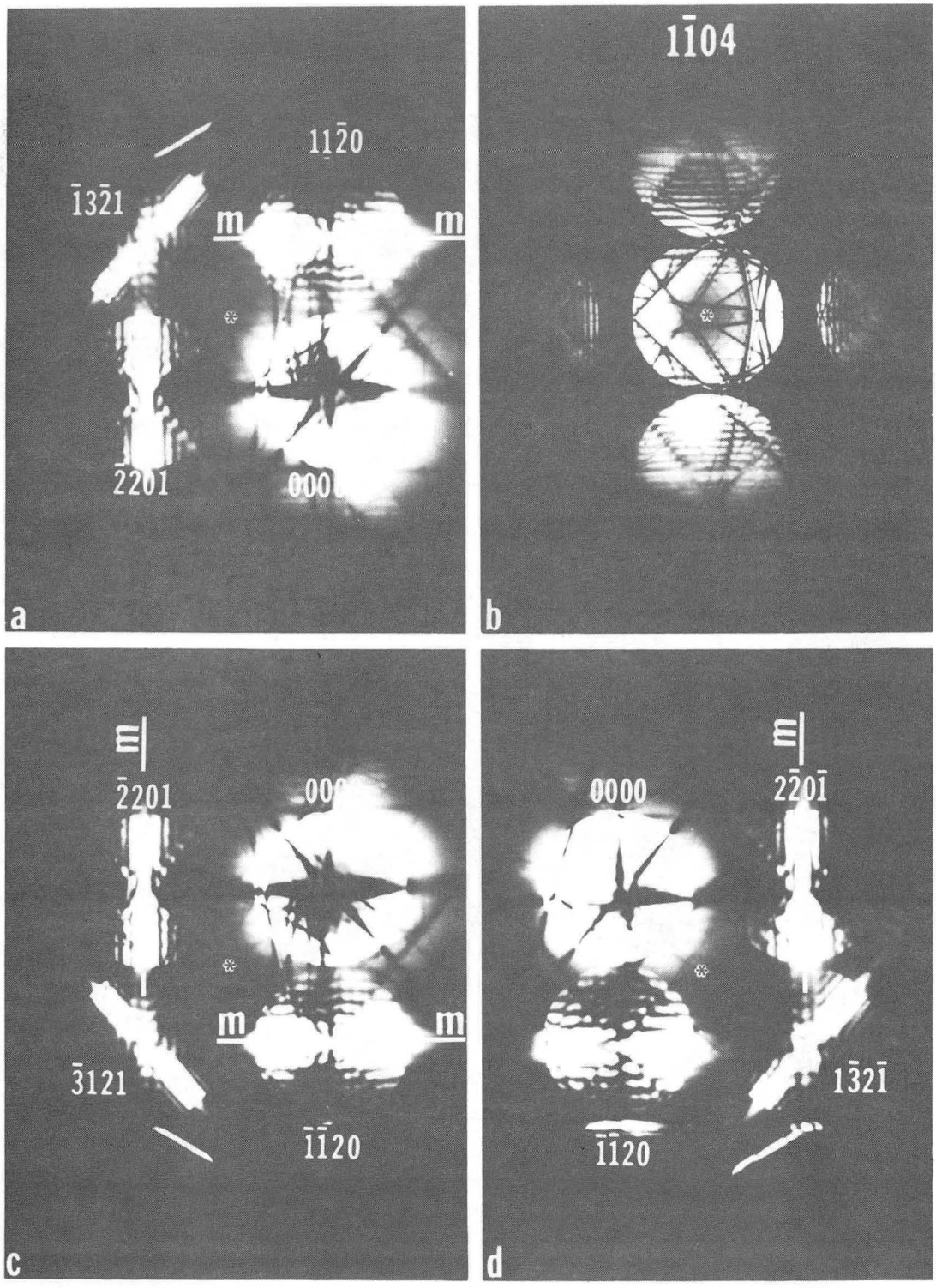

XBB 840-7656

Fig. 5

XBB 840-7663 A

Fig. 6

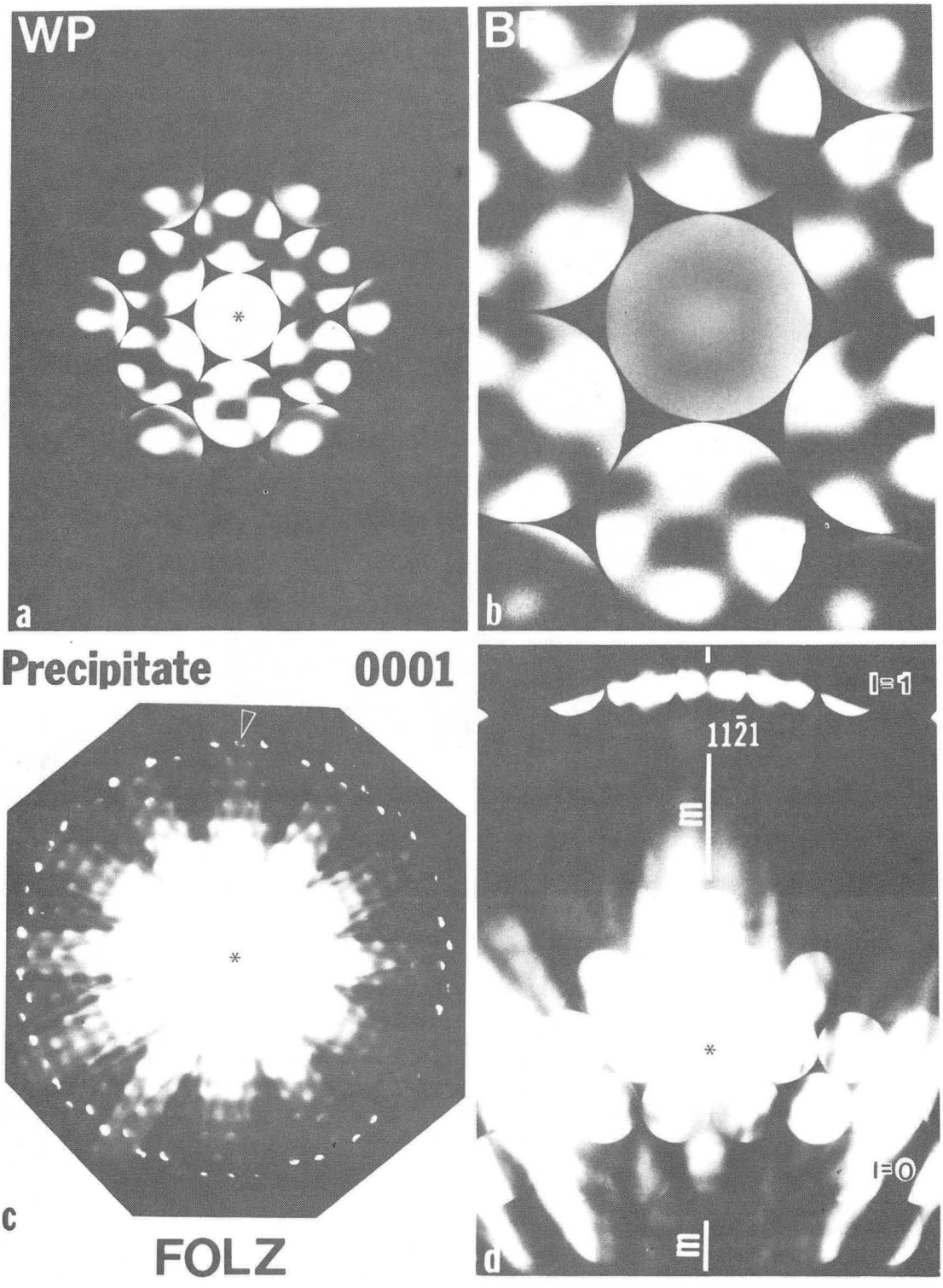

XBB 840-7661

Fig. 7

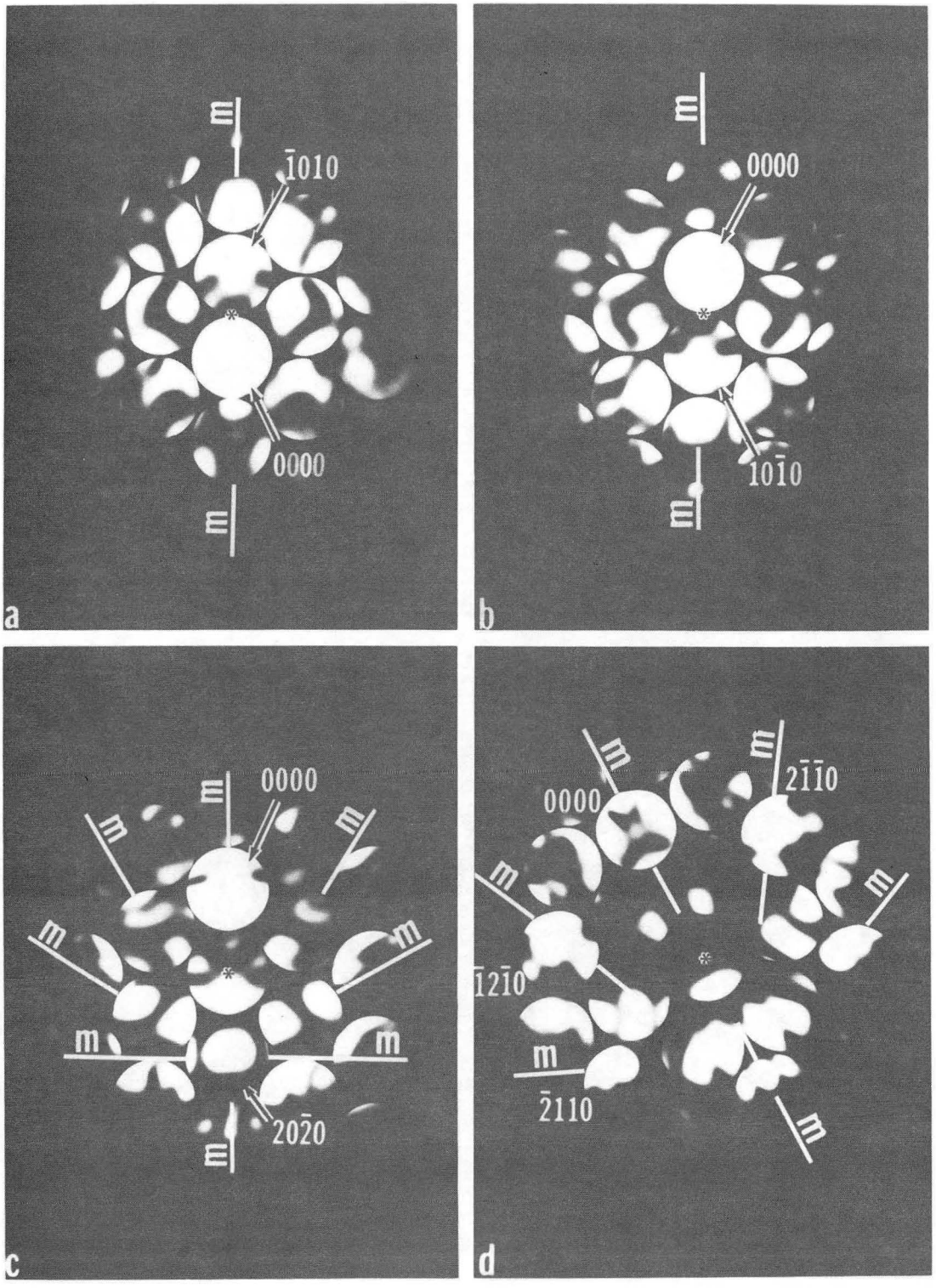

XBB 840-7659

Fig. 8

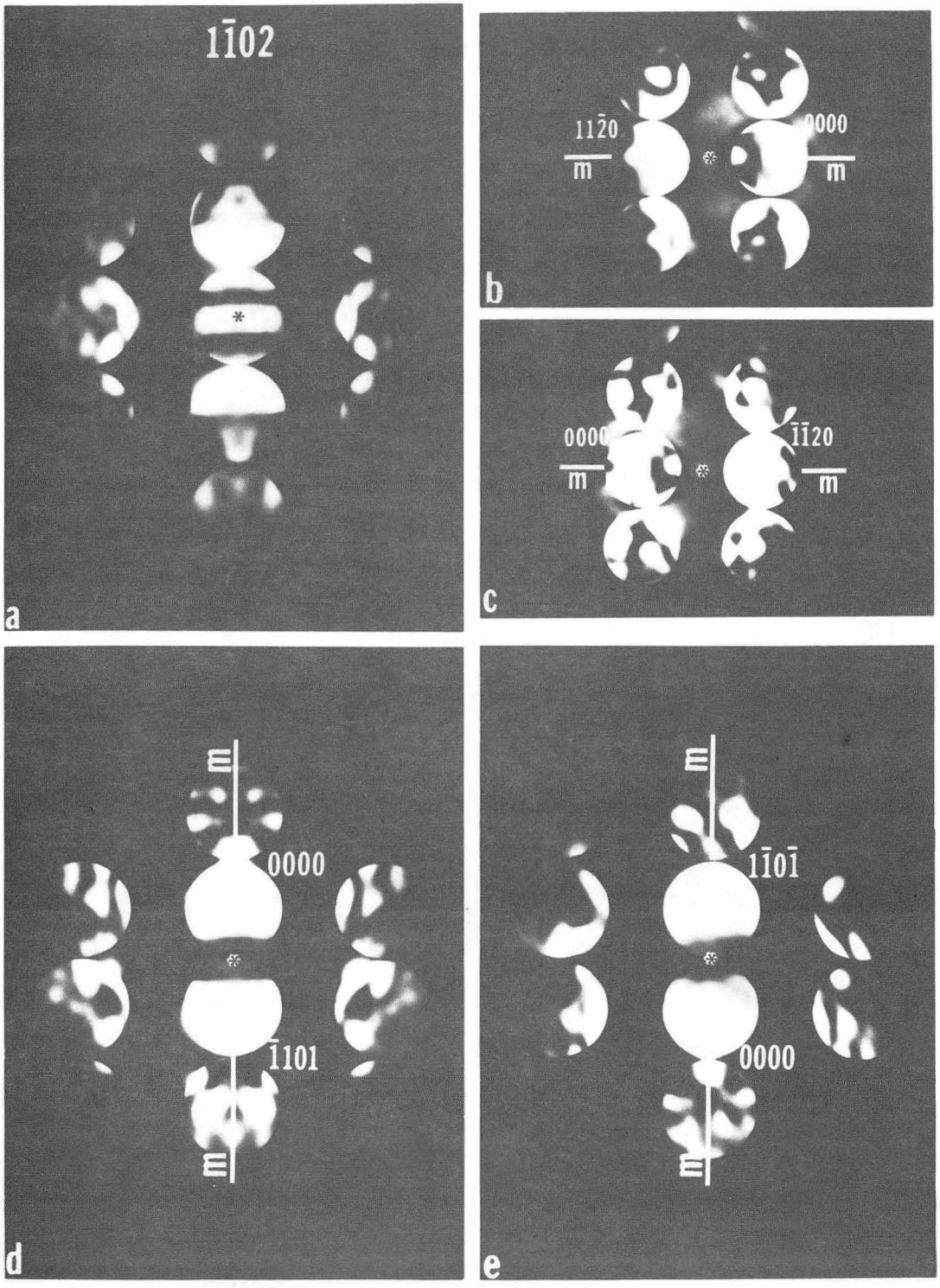

XBB 840-7660

Fig. 9

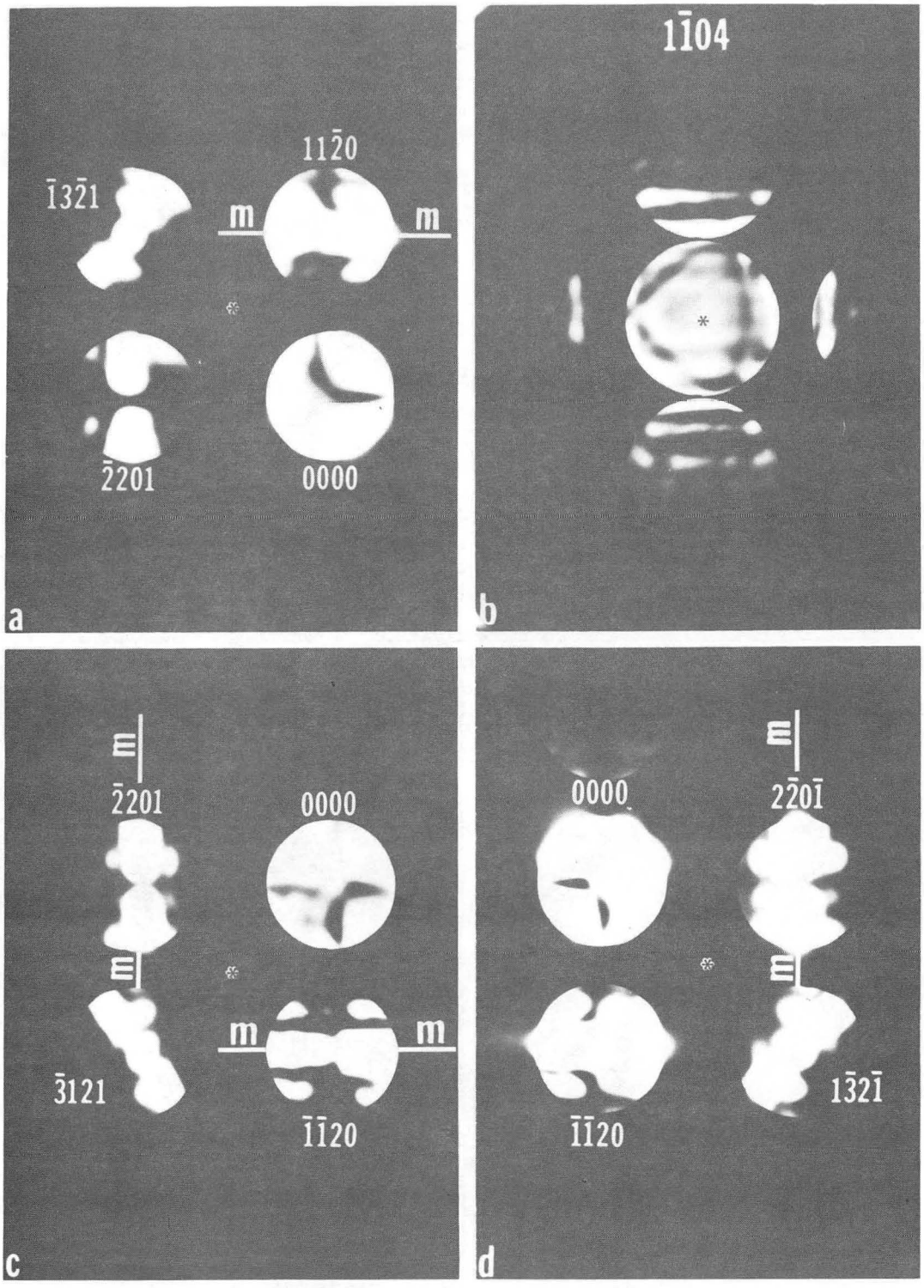

XBB 840-7657

Fig. 10

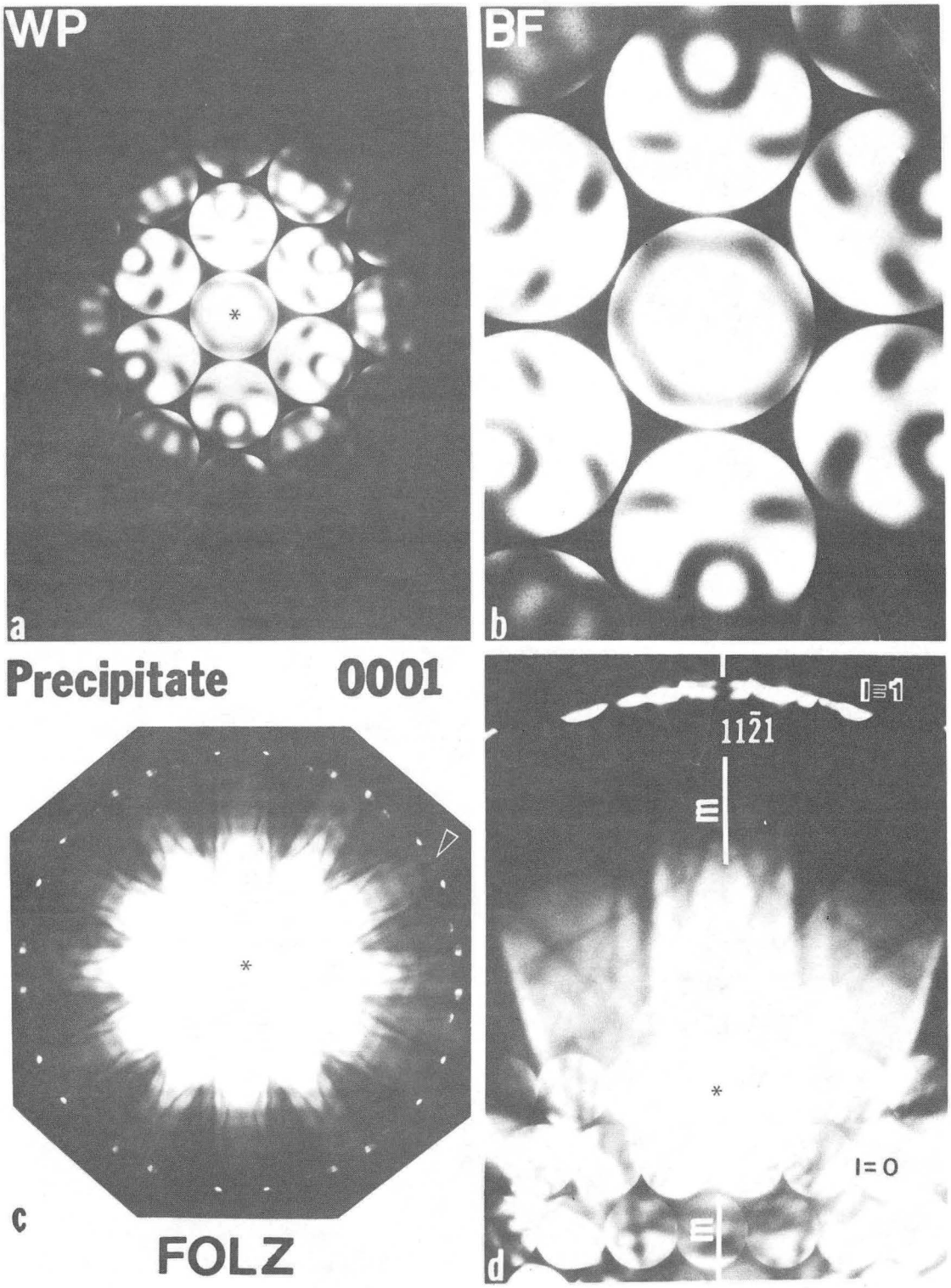

XBB 852-1543

Fig. 11

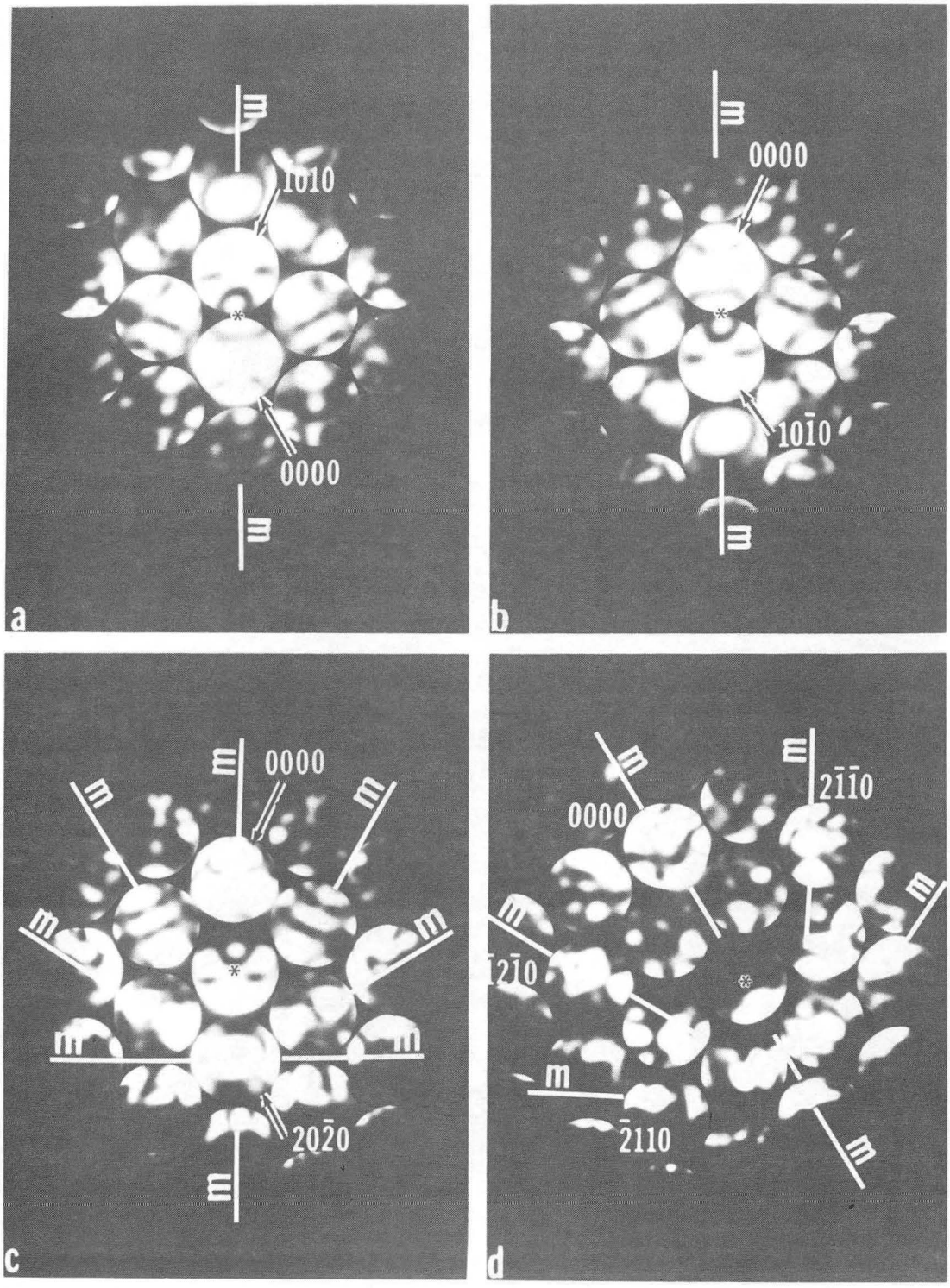

XBB 852-1542

Fig. 12

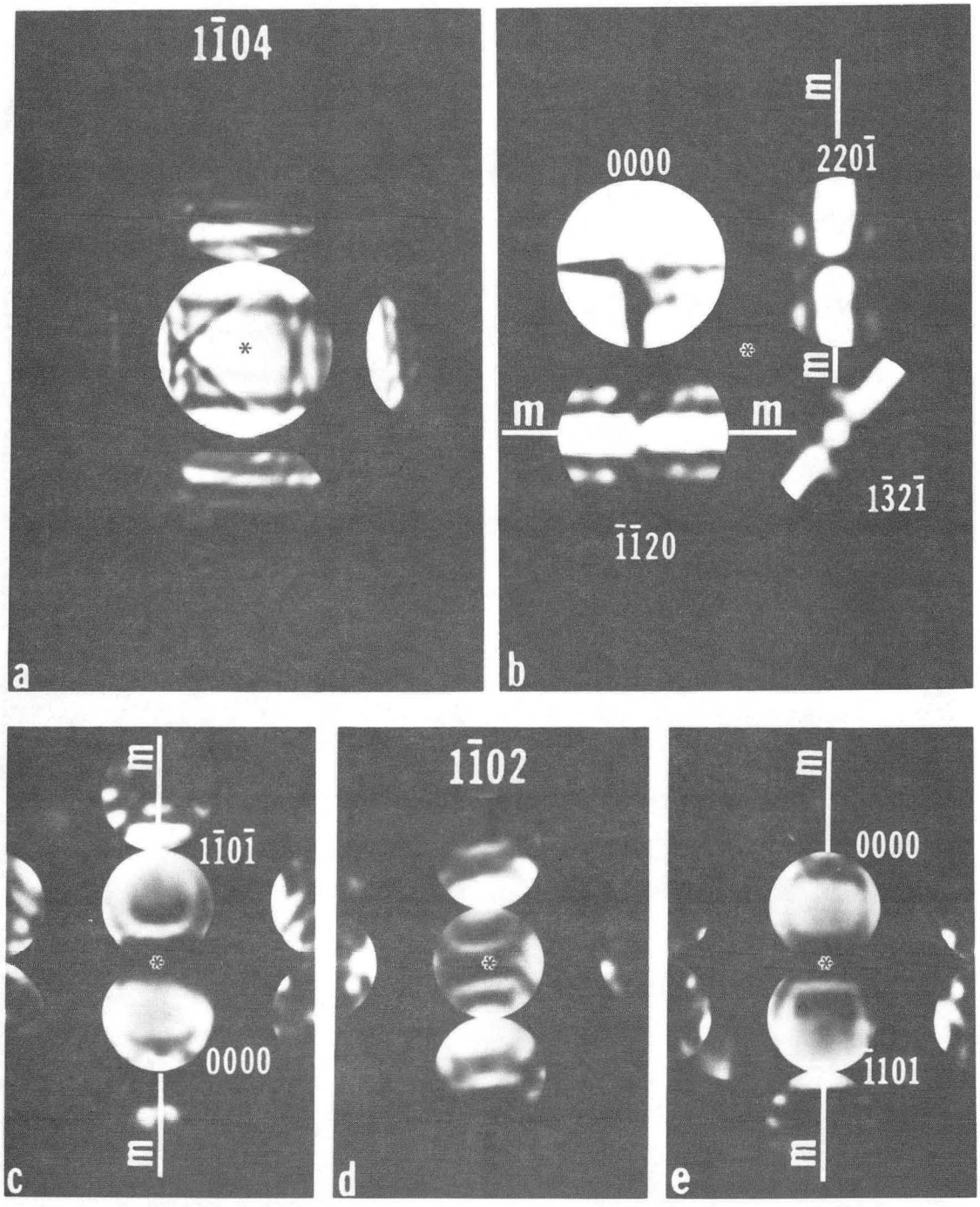

XBB 852-1541

Fig. 13

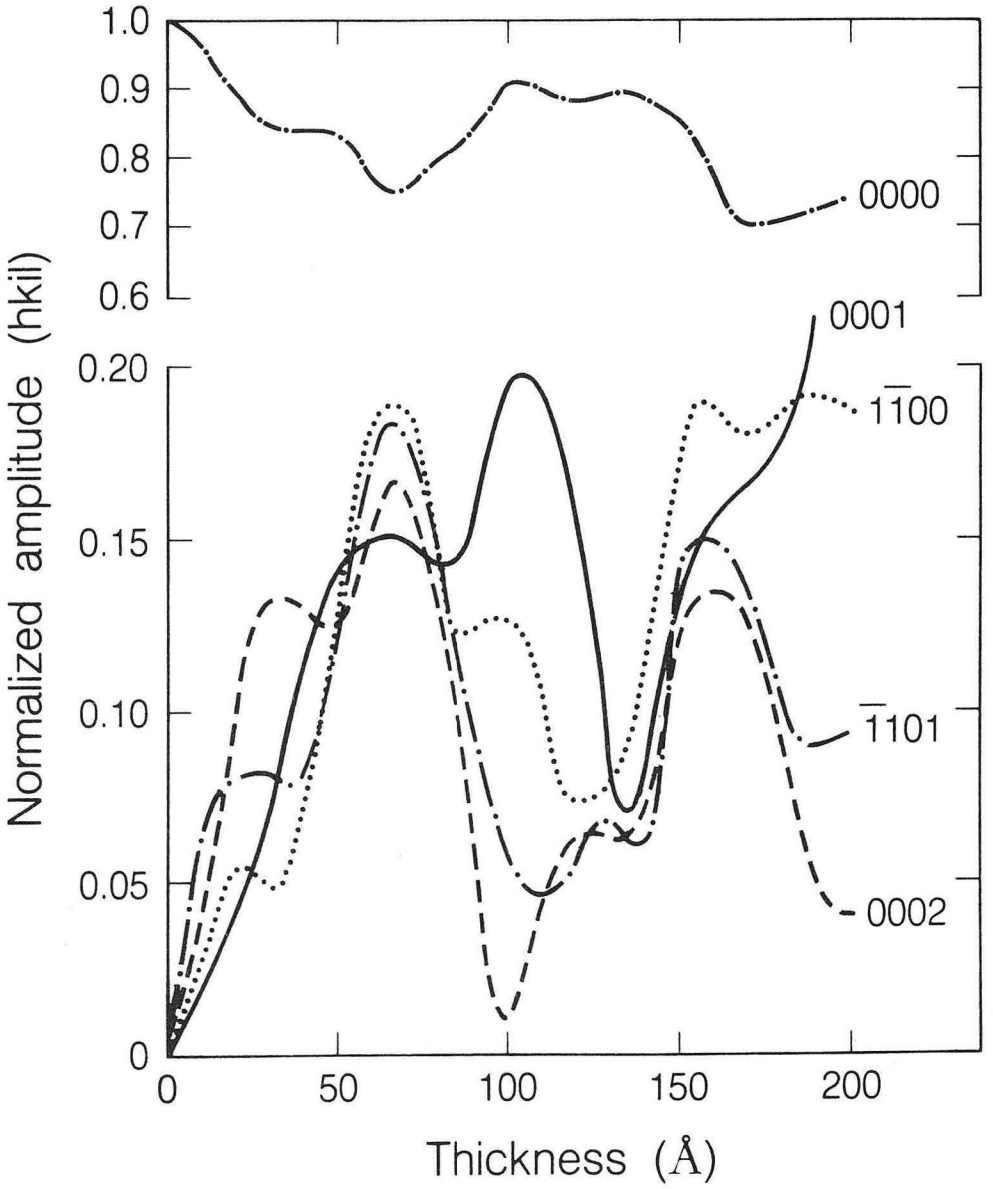

XBL 852-9755

Fig. 14

This report was done with support from the Department of Energy. Any conclusions or opinions expressed in this report represent solely those of the author(s) and not necessarily those of The Regents of the University of California, the Lawrence Berkeley Laboratory or the Department of Energy.

Reference to a company or product name does not imply approval or recommendation of the product by the University of California or the U.S. Department of Energy to the exclusion of others that may be suitable.

LAWRENCE BERKELEY LABORATORY
TECHNICAL INFORMATION DEPARTMENT
UNIVERSITY OF CALIFORNIA
BERKELEY, CALIFORNIA 94720